Nanofiber-Based Delivery of Therapeutic Peptides to the Brain

Mariarosa Mazza,[†] Rebecca Notman,[‡] Jamshed Anwar,[§] Alison Rodger,[‡] Matthew Hicks,[‡] Gary Parkinson,[†] Dave McCarthy,[†] Tina Daviter,[⊥] Julian Moger,[∥] Natalie Garrett,[∥] Tania Mead,[¶] Michael Briggs,[¶] Andreas G. Schätzlein,[†] and Ijeoma F. Uchegbu[†,*]

[†]UCL School of Pharmacy, 29−39 Brunswick Square, London WC1N 1AX, United Kingdom, [‡]Department of Chemistry and Centre for Scientific Computing, University of Warwick, Coventry CV4 7AL, United Kingdom, [§]Computational Biophysics Laboratory, Institute of Life Sciences Research, University of Bradford, Yorkshire BD7 1DP, United Kingdom, [⊥]Biophysics Centre, Institute of Structural and Molecular Biology and Department of Biological Sciences, Birkbeck, University of London, London WC1E 7HX, United Kingdom, [∥]School of Physics, University of Exeter, Stocker Road, Exeter EX4 4QL, United Kingdom, and [¶]GlaxoSmithKline, Pharmaceuticals R&D, Medicines Research Centre, Gunnels Wood Road, Stevenage SG1 2NY, United Kingdom

ABSTRACT The delivery of therapeutic peptides and proteins to the central nervous system is the biggest challenge when developing effective neuropharmaceuticals. The central issue is that the blood-brain barrier is impermeable to most molecules. Here we demonstrate the concept of employing an amphiphilic derivative of a peptide to deliver the peptide into the brain. The key to success is that the amphiphilic peptide should by design self-assemble into nanofibers wherein the active peptide epitope is tightly wrapped around the nanofiber core. The nanofiber form appears to protect the amphiphilic peptide from degradation while in the plasma, and the amphiphilic nature of the peptide promotes its transport across the blood-brain barrier. Therapeutic brain levels of the amphiphilic peptide are achieved with this strategy, compared with the absence of detectable peptide in the brain and the consequent lack of a therapeutic response when the underivatized peptide is administered.

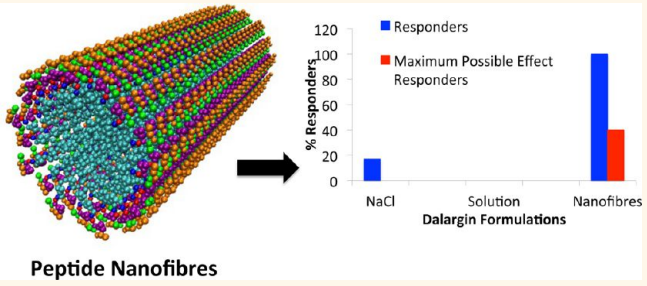

KEYWORDS: peptide brain delivery · blood-brain barrier · dalargin · palmitoyl dalargin · nanofibers · self-assembly

Delivery of therapeutic peptides to the central nervous system (CNS) remains a challenge to the development of effective neuropharmaceuticals. The central issue is that the blood-brain barrier (BBB), the interface between the blood and brain, is not permeable to large hydrophilic molecules.[1] Potential therapeutic peptides include amyloid beta aggregation inhibitors for Alzheimer's disease,[2] peptides for Parkinson's disease,[3] and analgesic neuropeptides,[4] but to date, these remain undeveloped because of the delivery challenges that include exclusion from the brain and degradation within the blood. Furthermore, the incidence of neurological diseases is predicted to rise,[5] making the demand for neurological therapies even more acute.

Various strategies have been attempted to enable drug compounds to cross the blood-brain barrier, following intravenous administration, including drug−ligand/antibody conjugates to exploit the endogenous transporters at the luminal side of the brain endothelial cells,[6−10] the inhibition of the brain ABC efflux transporters (P-glycoprotein[11] and breast cancer resistance protein[12]), the use of surfactant-coated poly(butylcyanoacrylate) nanoparticles,[13] and the use of cationic cell-penetrating peptides to effect adsorptive-mediated transcytosis.[14] Along with these intravenous injection approaches, there have evolved a number of intracranial strategies such as the use of brain implants following surgery,[15] convection enhanced infusions, in which catheters are placed at or close to the site of pathology in the brain,[16] and the popular Ommaya reservoir, in which a reservoir is placed under the scalp to deliver drug *via* a catheter intraventricularly.[17] Finally, there are also methods which simply involve the use of compounds which temporarily disrupt the blood-brain barrier (*e.g.*, the intracarotid infusion of mannitol or bradykinin analogues).[18]

* Address correspondence to ijeoma.uchegbu@ucl.ac.uk.

Received for review August 6, 2012 and accepted January 4, 2013.

Published online January 04, 2013
10.1021/nn305193d

For the brain delivery of peptides, approaches have been largely restricted to the chemical derivatization of these molecules in order to make them more lipophilic, less prone to hydrogen bonding in the blood, and more likely to traverse the lipid endothelial cell membranes. As such, the dimethylation of the tyrosine residue in D-pen^2-D-pen^5-enkephalin,[19] chlorination of the phenylalanine unit in D-pen^2-D-pen^5-enkephalin,[20] or use of lipid prodrugs of D-Ala^2-D-Leu^5 enkephalin (*e.g.*, formation of the C-terminal cholesteryl ester and N-terminal amidation with 1,4-dihydrotrigonelline)[21] have all been attempted. However, increasing a drug's lipophilicity sometimes results in increased plasma clearance and ultimately reduced brain exposure,[22] and so the use of lipidization alone is not without its drawbacks. Other methods that have been used to deliver peptides include methods to increase enzyme stability such as the use of cyclic peptides, for example, the cyclic peptide D-pen^2-D-pen^5-enkephalin.[23] As there are no neuropeptide drugs on the market, it is clear that all of these strategies have met with limited success.

Here we present a peptide brain delivery strategy using peptide drug nanofibers as a concept and show that self-assembling peptide drugs, which give rise to nanofibers, are able to deliver the model peptide dalargin to the brain and elicit a pharmacological response. Dalargin is usually excluded from the brain. A key feature of these drug nanofibers is the fact that the peptide chains in the peptide nanofibers are wrapped tightly around the nanofiber core, a feature which would prevent the degradation of these peptides *in vivo*. Peptide nanofibers have been investigated for tissue and nerve regeneration[24,25] and explored *in vitro* as cell antiproliferative agents,[26] but they have not been used to deliver drugs across the blood-brain barrier.

RESULTS AND DISCUSSION

To demonstrate the concept of using an amphiphilic derivative of a peptide to enhance its delivery to the brain, we employed the model peptide dalargin (Tyr-D-Ala-Gly-Phe-Leu-Arg), an opioid receptor agonist, which shows specificity for the mu opioid receptors,[27] and which is normally excluded from the central nervous system (CNS). The amphiphilic derivative of dalargin, palmitoyl dalargin (pDal), was synthesized using fluorenylmethyloxycarbonyl chloride (Fmoc)-based chemistry, in which synthesis of the peptide is followed by the linking of a palmitoyl moiety to the tyrosine hydroxyl *via* an ester link. It is envisaged that this amphiphilic peptide derivative would give rise to the drug dalargin on encountering endogenous esterases, in a similar manner to the release of leucine^5-enkephalin from the cleavage of tyrosine^1-palmitate-leucine^5-enkephalin (TPLENK).[28] The resulting peptide bears a positively charged (at physiological pH) arginine at one end and a long alkyl chain at the opposite end (Figure 1a).

The pDal is able to self-assemble into high axial ratio micellar aggregates. Self-assembly of an aqueous dispersion of pDal (1 mg mL^{-1}) was induced by probe sonication. Peptide nanofiber transmission electron micrographs (Figure 1b) reveal two distinct morphologies, twisted or straight elongated micellar aggregates. The twisted elongated nanostructures resemble the fibrils observed for glucagon amyloid fibrils, where two or more protofilaments twist repetitively around each other.[29] Mixed populations of straight and twisted nanofibers have previously been noticed for amyloids derived from bovine insulin fibrils.[30]

We administered intravenously pDal nanofibers in NaCl (0.9% w/v) and dalargin alone in NaCl to groups of mice (n = 5) at a dalargin dose of 30 mg kg^{-1} and measured peptide levels in the plasma, brain, and liver (Figure 2) using liquid chromatography−mass spectrometry (LC−MS), which is the method of choice for monitoring peptide distribution in biological matrices.[31,32] Dalargin was not detected in the brain, liver, or plasma when either dalargin or pDal was administered intravenously, and only dalargin's main metabolite, D-Ala^2-Leu^5-enkephalin, was detected in the plasma after administering dalargin or pDal nanofibers (Figure 2b). Metabolite analysis was focused on the main metabolite as D-Ala^2-Leu^5-enkephalin has weak opioid activity.[33] In contrast, pDal was detectable in all tissue samples analyzed (Figure 2a,c,e) and more crucially detected in the brain for up to 4 h after intravenous administration (Figure 2c). Brain levels of pDal with respect to the plasma increased steadily for up to 90 min, evidence of a slower clearance of pDal from the brain and that brain pDal levels recorded are not due to the levels in the brain vasculature (Figure 2d). Further evidence that the brain levels identified are in the brain parenchyma, as opposed to brain vascular volume, is drawn from the fact that the vascular volume has been estimated at 12 μL g^{-1},[34] hence, a calculation of the pDal concentration within the theoretical brain vascular volume reveals that the vascular volume (plasma) levels contributed 11% at the 3 min time point, 5% at the 10 min time point, and 1% or less at the later time points. The brain concentration actually exceeds the plasma concentration at the 90 min time point (Figure 2a inset and Figure 2c). Liver levels of pDal also increased steadily with respect to the plasma levels (Supporting Information Figure SI 9), evidence that liver clearance was also delayed relative to plasma clearance. D-Ala^2-Leu^5-enkephalin was detected in the plasma after the intravenous administration of pDal, indicative of the formation of dalargin from pDal (Figure 2b). We thus surmise that pDal is converted to dalargin *in vivo* by plasma esterases in a similar manner to the conversion of TPLENK to leucine^5-enkephalin in the plasma and liver.[28] Dalargin tissue levels are below the limit of

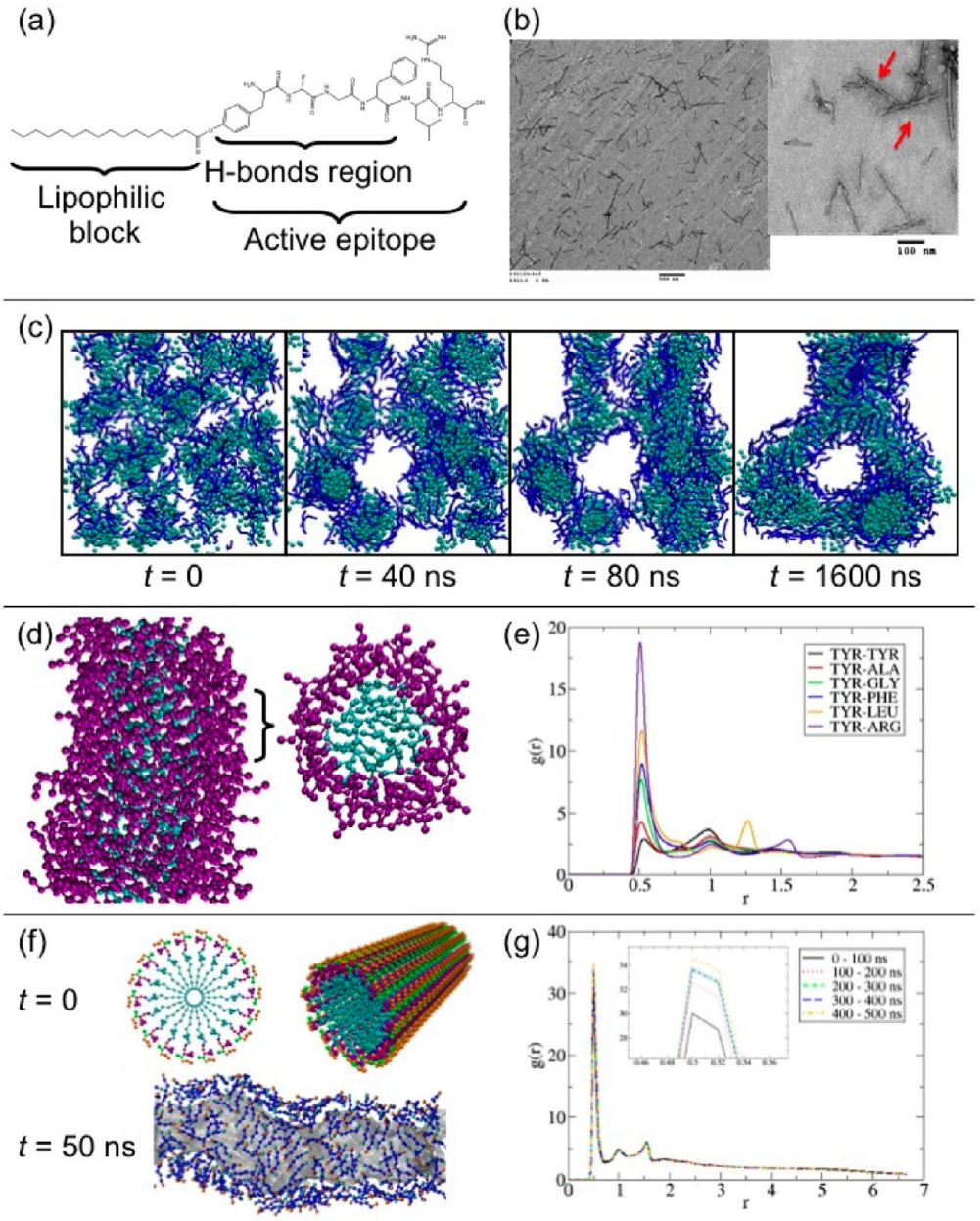

Figure 1. (a) pDal molecular structure; (b) cylindrical and twisted nanofibers as seen using TEM (red arrows indicate twisted nanofibers); (c) snapshots from molecular simulations of the self-assembly of pDal nanofibers starting from a random configuration; (d) 2 nm length cross section of the nanofiber formed during simulation, revealing the wrapping around of the peptide moiety (shown in purple) around the fiber axis; the hydrophobic core shown in cyan; (e) pairwise radial distribution function for the TYR backbone bead with respect to all other amino acid backbone beads in a nanofiber; (f) idealized nanofiber structure as previously proposed by others (t = 0), with the pDal molecules arranged so that the peptide fragment extends radially outward from a hydrophobic core, and the converged molecular structure of the nanofiber after 50 ns simulation time (t = 50). The converged structure shows wrapping around of the peptide moiety about the fiber axis. The hydrophobic core is colored gray; peptide backbone particles are shown in blue with the arginine backbone particle in orange and the tyrosine backbone particle in cyan. Side chain and solvent particles have been removed for clarity. (g) Pairwise radial distribution function $g(r)$ between the ARG backbone bead and the TYR backbone bead, calculated over five different time periods of the simulation.

quantification (50 ng mL^{-1} in plasma and 150 ng mL^{-1} in the brain) as the species is so short-lived and is not even detected when dalargin is injected intravenously (Figure 2a−c,e).

To provide further evidence that the peptide nanofiber formulations did indeed cross the blood-brain barrier, we employed coherent anti-Stokes Raman scattering (CARS) microscopy. CARS microscopy was used to visualize pDal fibers within the brain parenchyma without the need to modify the fibers with fluorescent labeling. Fluorescent labeling causes chemical perturbation that could influence transport of the drug across the BBB. Moreover, the technique provided nondestructive visualization of the surrounding brain tissue

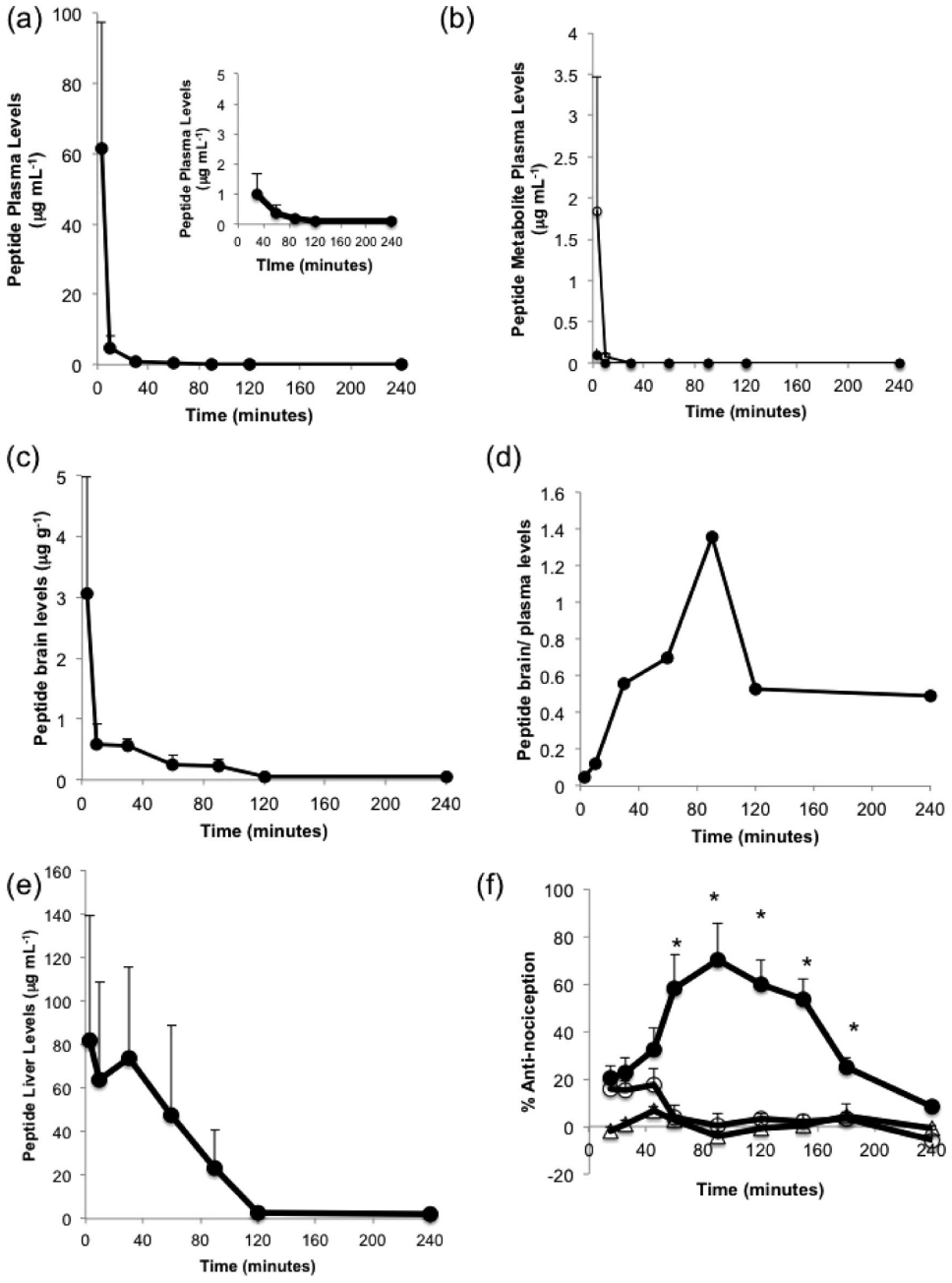

Figure 2. (a) Pharmacokinetic (mean ± sd) and pharmacodynamic (mean ± sem) profiles of pDal nanofiber and dalargin formulations after intravenous administration: mice ($n = 5$) received a dose of 30 mg kg^{-1} of dalargin either as dalargin or pDal nanofibers and dissolved or dispersed in NaCl (0.9% w/v), respectively. Analyses were carried out using LC−MS, and dalargin was not detected in any of the samples after the administration of dalargin or pDal. (a) pDal plasma levels expressed in μg mL^{-1} (inset pDal plasma levels at the later time points, from 30 min after dosing, enlarged for clarity). (b) D-Ala^2-Leu^5-enkephalin (dalargin metabolite) plasma levels following the intravenous administration of dalargin (○) or pDal nanofibers (●); (c) pDal brain levels expressed in μg g^{-1}; (d) pDal brain/plasma ratio following the intravenous injection of pDal nanofibers (mean pDal brain/mean pDal plasma); (e) pDal liver levels expressed in μg g^{-1}. (f) Pharmacodynamic evaluation of dalargin and pDal nanofiber formulations presented as % anti-nociception in the tail flick bioassay when mice were administered sodium chloride (0.9% w/v, △), dalargin solution in NaCl (15 mg kg^{-1}, ○), or pDal nanofibers in NaCl (15 mg kg^{-1}, ●), * = statistically significant difference between pDal nanofibers and dalargin groups ($p < 0.05$). The baseline latency ranged from 1.84 ± 0.24 to 2.14 ± 0.54 s, and the maximum time of observation was 10 s.

structures to confirm the location of the fibers in relation to the BBB. CARS microscopy is a label-free imaging technique that provides real-time imaging of intact tissues with subcellular spatial resolution based on molecular vibrational spectroscopy.[35] A coherent nonlinear Raman signal is generated by focusing two synchronized ultrafast pulse trains into a sample with a difference in frequency matched to a Raman-active mode of a molecular species of interest. The nonlinear nature of the process confines the signal to a

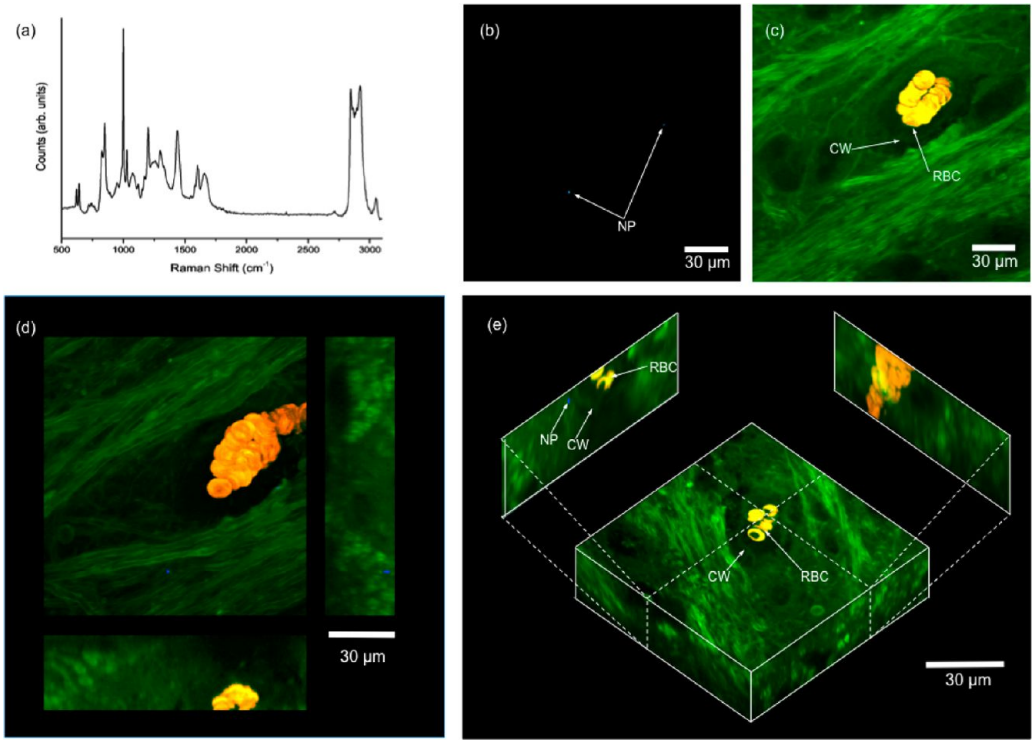

Figure 3. (a) Spontaneous Raman spectrum of the pDal nanofibers. (b–e) *Ex vivo* CARS images of brain tissue of a male CD-1 mouse 30 min following a 30 mg kg^{-1} IV dose of pDal nanofibers. (b) Epi-CARS image demonstrating the high contrast derived from the abundant CH_2 stretching mode at 2850 cm^{-1} of the nanoparticles (NP). (c) Merger of NL-PTL (yellow) and SRS (green) images of the same region of tissue shown in (b), which provided label-free contrast of red blood cells (RBC), the surrounding capillary wall (CW), and brain tissue structures. (d,e) Multiplanar and maximum intensity projections of a 30 μm deep image stack in the region of the blood vessel (RBC = red blood cells).

submicrometer focus that can be scanned in space, allowing three-dimensional mapping of biomolecules in tissue with subcellular resolution. As we have previously shown,[36−38] the technique has exceptional capabilities for locating nanomedicines within tissues with 3D subcellular resolution. The directional nature of the signal produced in CARS microscopy has particular use for detecting nanoparticles against a background of biological tissues. Due to the coherent nature of the CARS process, the spatial distribution of the emitted signal is more complicated than that observed for incoherent microscopy techniques, such as fluorescence, where the signal is emitted in all directions. In CARS microscopy, the direction in which the signal is emitted can vary depending upon the size of the scattering object. For CARS generated in bulk tissues, the constructive interference occurs in the forward direction, resulting in a forward propagating signal, and in the backward direction, destructive interference leads to no epi-CARS signal from bulk objects. Conversely, the CARS signal generated by objects within the focal volume, whose size is insufficient for complete destructive interference in the epi-direction to occur, will propagate equally in the forward and epi-directions. This criterion is fulfilled by particles smaller than one-third of the pump beam wavelength, which for the typical excitation wavelengths used corresponds to objects smaller than approximately 300 nm. The forward propagating signal from these particles is often swamped by the strong forward CARS signal from bulk media. However, the epi-signal, which has minimal contribution from bulk media, provides high contrast of small scatters. For polymeric particles, this effect is compounded by the fact that the CARS signal intensity scales quadratically with the number of resonant bonds within the sample volume, and the high bond repetition within the particles leads to extremely strong signals. The combination of these phenomena provides a highly effective mechanism to separate the signal from polymeric nanomaterials and the surrounding biological tissues in which they are situated.

CARS contrast of the pDal nanofibers was derived from the CH_2 stretch mode at 2850 cm^{-1}, which is abundant in the palmitoyl group and clearly visible in the spontaneous Raman spectrum of the nanofibers shown in Figure 3a. Since the CARS signal intensity scales quadratically with the number of resonant bonds within the sample volume, this mode provided excellent contrast of the nanofibers against the background of biological structures. Figure 3b–e shows *ex vivo* CARS images of brain tissue of a male CD-1 mouse 30 min following an intravenous dose (30 mg kg^{-1}) of pDal nanofibers. Figure 3b illustrates the contrast of the particles that could be achieved using epi-CARS

detection. Although some autofluorescence within the tissue was present in the epi-CARS images, it is several standard deviations weaker than the intense pDal signal and may be efficiently thresholded out of the images. Control samples devoid of nanoparticles imaged under the same conditions showed no epi-CARS signal above the threshold value. Figure 3c demonstrates how the combination of nonlinear photothermal lensing (NP-PTL, yellow) and spontaneous Raman scattering (SRS, green) provided label-free contrast of blood vessels and the surrounding cellular structures, respectively. The presence of red blood cells in the upper half of the image indicates that the image plane passed through a microvessel (approximately 14 μm in diameter). Since all three images (epi-CARS, SRS, and NP-PTL) are acquired simultaneously using the same excitation, all three images are perfectly co-registered with no positional error and may be merged to determine the location of the nanofibers with respect to the BBB. Figure 3d,e shows multiplanar and maximum intensity projections of a 30 μm deep image stack acquired at a 3$\times$ zoom centered on the region containing the blood vessel. The epi-CARS signal from the pDal (blue) is present both in the BBB vessel and the brain tissue. These figures show that pDal is clearly located in the brain parenchyma, which was confirmed by the LC–MS data. Since epi-CARS signals with sufficient intensity to appear above the image threshold can only occur from nanoscale objects containing a high density of the palmitoyl groups, these images confirm that intact nanofibers, rather than degraded polymer material, have crossed the BBB. Nanofibers have been shown to enter MT3T3-E1 cells by endocytosis[39] and have also been internalized by SKBR-3 cells in culture.[26] Additionally, particles have been reported to cross the BBB by receptor-mediated endocytosis for example[40] and by other nonspecific uptake mechanisms,[41] and although we have no evidence of receptor-mediated endocytosis, it is conceivable that the pDal nanofibers could have crossed the brain endothelial cells by endocytotic mechanisms.

In order to ascertain whether the administration of pDal does result in central pharmacodynamic effects, we also conducted the tail flick bioassay[28,38] in which animals are subjected to a thermal stimuli and the time required to remove the tail from the stimulus, used as a measure of anti-nociception. Only animals administered pDal nanofibers exhibited an anti-nociceptive response (Figure 2f), confirming that pDal from this delivery system crosses the blood-brain barrier to induce a pharmacodynamic response. The time for peak activity was delayed with respect to the peak brain levels of the pDal (which is in effect a prodrug of dalargin), indicating that the active species was actually the drug dalargin. Although dalargin was too short-lived/below the limit of quantification to be detected, the dalargin metabolite (D-alanine^2-leucine^5-enkephalin) was detected at the 5 min time point in the plasma after the intravenous administration of pDal nanofibers (Figure 2b), indicating that dalargin was generated *in vivo*. Our conclusion that the activity that we are seeing is due to the dalargin originating from the pDal nanofibers stems from the delayed response and the fact that we know that palmitoyl tyrosine ester prodrugs of leucine^5-enkephalin give rise to leucine^5-enkephalin *in vivo*.[28] Ester prodrugs are rapidly cleaved to the parent drug: being completely cleaved within 30 min in the case of the phosphate ester prodrug of the antifungal agent, ravuconazole,[42] or the (glycyl, glutamyl)-diethyl ester prodrug of the antitumor agent, *S*-(*N*-*p*-chlorophenyl-*N*-hydroxycarbamoyl)glutathione.[43] Additionally, it is also possible that the prolonged duration of activity of pDal nanofibers could indicate that the receptor–agonist dissociation kinetics are slow. A prolonged duration of action has been observed with mu opioid receptor antagonists[44] and agonists[45] when the receptor–antagonist/agonist dissociation kinetics are slow. Finally, we cannot rule out a contribution to the anti-nociceptive response by dalargin's main metabolite D-alanine^2-leucine^5-enkephalin (Figure 2b) as D-alanine^2-leucine^5-enkephalin is also an opioid receptor agonist.[33]

The above results clearly confirm that pDal is being delivered to the CNS in sufficient quantity to elicit a pharmacodynamic response, while dalargin itself is not detectable in the brain, plasma, or liver, being completely metabolized on arriving in the circulation. By contrast, pDal appears to overcome the main challenges that plague delivery of peptides to the CNS, namely, plasma degradation and exclusion from the brain by the blood-brain barrier. We infer that pDal's ability to form nanofibers that can persist in the blood circulation must offer the molecules stability to degradation. To investigate the reason for this plasma stability and peptide brain penetration, we attempted to elucidate the molecular organization of the nanofibers using linear dichroism (LD) and X-ray diffraction (XRD), complemented by molecular simulation.

Both linear dichroism and X-ray diffraction revealed that the nanofibers comprised predominantly β-sheets aligned along the long axis of the fibers, and that the tyrosine residues are located within the interior of the fiber while the alkyl groups are pointing perpendicular to the fiber's long axis. The LD spectrum (Figure 4) of a pDal nanofiber dispersion shows a maximum signal at $\sim$201 nm, indicating that the C=O groups are approximately parallel to the long axis of the fiber, and thus the β-sheets are parallel to the fiber axis. The two positive tyrosine peaks at 279 and 286 nm (Figure 4B) are shifted to a longer wavelength (normally expected to be at 275 nm), indicating that the tyrosine residues are located within the interior of the fiber.[46] The negative signal around 235 nm (Figure 4B) suggests that the transition moment along the *O*-alkyl group is pointing

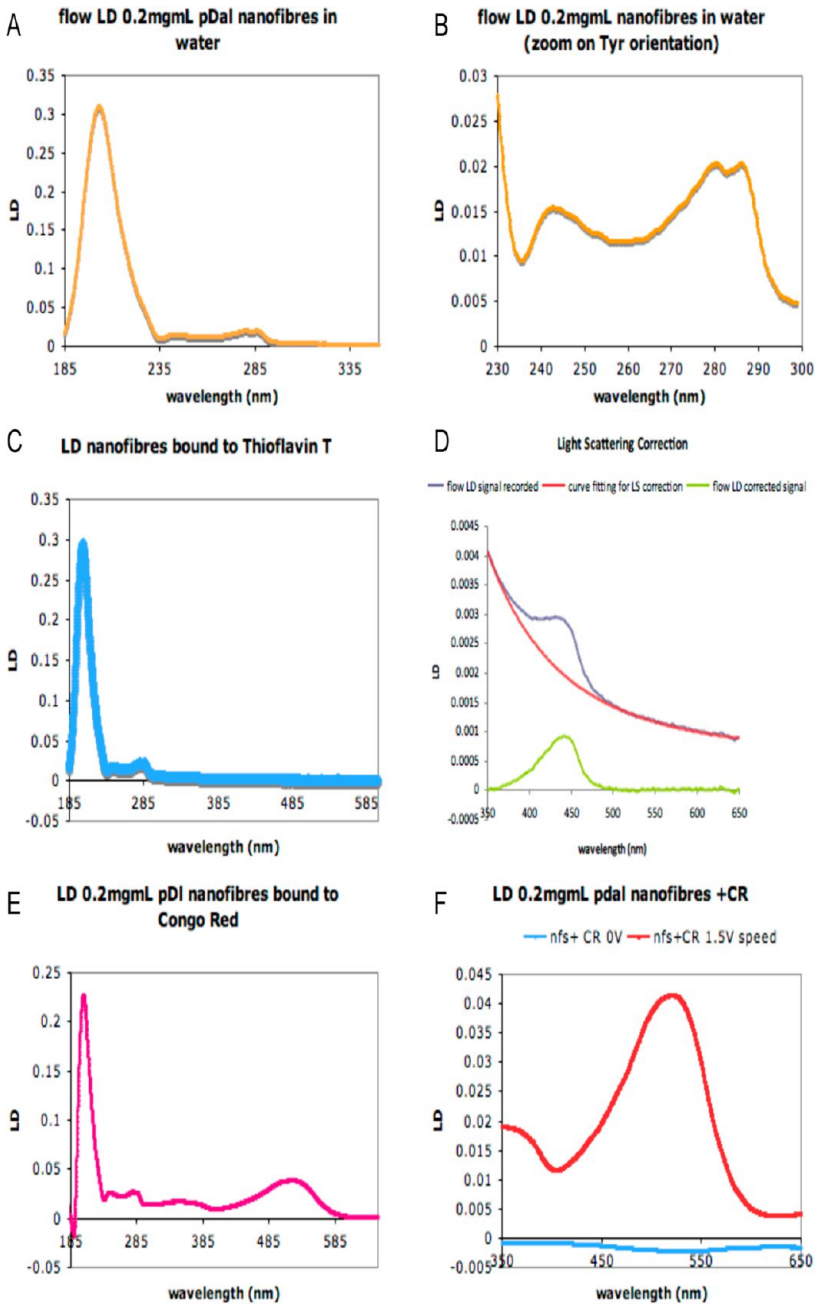

Figure 4. LD spectra of pDal nanofiber dispersions (0.2 mg mL^{-1}): (A) pDal nanofibers in water; (B) pDal nanofibers in water with a zoom at the 230−300 nm region. The two positive tyrosine peaks at 279 and 286 nm are shifted to a longer wavelength than would be expected for these moieties in aqueous media as we would normally expect a single peak at ∼275 nm, indicating that the tyrosine residues are located within the interior of the fiber. Additionally, there is also a negative signal around 235 nm, thus the transition moment along the *O*-alkyl group is pointing perpendicular to the fiber long axis. (C,D) pDal nanofibers in a solution of fluorescent thioflavin T (Th-T, 22 μM) in EDTA buffer (10 mM Tris-HCl, 1 mM disodium EDTA, pH 8.0). The sample is affected by light scattering, as can be deduced by the sloping baseline (D), hence we corrected the effect of the light scattering as reported in detail in the Supporting Information. (E,F) pDal nanofibers in a solution of Congo Red (CR, 10 μM) in PBS (5 mM, NaCl = 150 mM).

perpendicular to the fiber long axis.[46] It was also confirmed by fluorescent thioflavin T (22 μM) and Congo Red (10 μM) binding studies that the β-sheets were in a parallel arrangement to the fiber axis (Figure 4C−F). The X-ray diffraction carried out on a dried stalk of pDal nanofibers revealed a sharp meridional diffraction at 4.8 Å (Figure 5), which is the distance between adjacent α-carbon atoms in hydrogen-bonded β-strands in the β-sheet, thus further confirming the predominance of the β-sheet secondary structure parallel to the nanofiber axis.[47,48]

Molecular dynamics simulations were carried out using a coarse-grained representation of the pDal molecule. The system size comprised 512 molecules

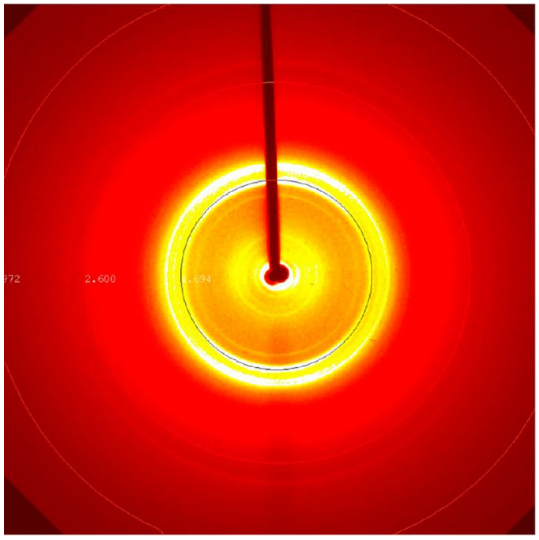

Figure 5. XRD of a dry stalk of pDal nanofibers.

of pDal with an equal number of chloride counterions (required to neutralize the charge) randomly inserted in water. Simulations were carried out over a range of pDal: water particle ratios 1:10, 1:20, 1:25, and 1:50 (each water particle represented four water molecules), covering a wide range of pDal concentrations. In all simulations, pDal molecules self-assembled into fiber-like structures that persisted for the entire simulation (1.6 μs). A series of snapshots showing the simulated self-assembly of pDal molecules for the 1:50 concentration system are presented in Figure 1c. The pDal molecules aggregate into small clusters, which then associate over ~100 ns to form long fiber-like structures. In the simulation presented here (Figure 1c–e), two nanofibers formed spontaneously, lying parallel to each other and spanning the periodic box. A snapshot showing a cross section of one of the nanofibers is shown in Figure 1d. It is clear that the peptide backbone (magenta-colored particles) wraps around and lines the exterior of the fiber while the alkyl chains cluster together to form a hydrophobic core (cyan-colored particles). The alkyl chains lie perpendicular to the long axis of the nanofiber, pointing toward the center of the nanofiber. There is also significant tyrosine–arginine interaction, indicative of an overall preference for an antiparallel alignment of the peptide moieties. The observed wrapping around of the peptide backbone about the hydrophobic core is quite distinct from the cylindrical micelle-like structure that is generally thought to characterize the structure of amphiphilic peptide nanofibers.[49,50] In the latter, the peptide fragments extend out radially from the core, forming a halo, rather than wrapping round the core. To address the possibility of pDal existing in such a structure, we simulated an idealized, cylindrical micelle-like structure with extended peptide chains of pDal in water. The idealized structure rapidly converged to the wrap-around structure observed in the self-assembly simulations (Figure 1f).

CONCLUSIONS

We conclude from the experiments and the simulations that pDal nanofibers consist of a central hydrophobic core surrounded by wrapped-around peptide β-sheets (Figure 1d,f). Given such a structure, we conclude that the tight wrapping around of the peptide moieties makes the nanofibers less prone to dissolution in the plasma and would also protect the peptide bonds from degradation. Had the structure been more akin to a cylindrical micelle with the peptide moieties pointing out radially, the peptide linkages would be more accessible and prone to degradation. Being less susceptible to degradation, one would expect the current nanofibers to persist in the plasma, making them available at the blood-brain barrier. The CARS data suggest the presence of pDal aggregates, possibly nanofibers, within the brain parenchyma, and it is possible that pDal nanofibers are taken up by endothelial cell endocytosis. However, we are unsure how much of the brain pDal is made up of nanofibers and how much is made up of pDal molecules as there is a possibility of the nanofibers disassembling in close proximity to the endothelial cell membrane and absorption then taking place on a molecular basis.

Summarizing, we have demonstrated the concept of using an amphipathic derivative of a peptide that self-assembles into nanofibers to deliver the peptide to the central nervous system. The nanofiber with the peptide backbone tightly wrapped around the fiber core appears to protect the peptide from plasma degradation.

METHODS

Peptide Synthesis. The peptide was synthesized by Peptisyntha (Torrance, California, USA) and a batch by us. Briefly, to the H-Arg(Pbf)-2-Cl-Trt resin (0.943g, 0.53 mmol g^{-1}) was added dimethyl formamide (DMF, 4–8 mL), and the resin was left to swell for 1 h. To the swollen resin was then added a solution of DMF containing the Fmoc (fluorenylmethyloxycarbonyl chloride) amino acid (Fmoc-L-leucine, 0.44 g, 1.25 mmol), *O*-(1*H*-benzotriazole-1-yl)-*N*,*N*,*N*′,*N*′-tetramethyluronium hexafluorophosphate (HBTU, 0.47 g, 2.5 mmol), and 1-hydroxybenzotriazole (HOBt, 0.436 mL, 2.5 mmol). To the reaction was then added *N*,*N*-diisopropylethylamine (DIEA, 191 mg, 2.5 mmol), and the reaction was allowed to proceed for 30 min. For each amino acid residue coupled, the above procedure was performed twice. After coupling each residue, the Kaiser test was performed to ensure coupling was complete. Deprotection of the Fmoc moiety after washing the resin with DMF (150 mL) was achieved by adding piperidine (20% v/v in DMF, 10 mL) to the resin beads, which were then agitated for 10 min (performed twice). The process detailed above was repeated until synthesis of Fmoc-Tyr-D-Ala-Gly-Phe-Leu-Arg was complete. All peptide synthesis steps were performed at room temperature. Once peptide

synthesis had been completed, the resin was washed with DMF (250 mL), followed by dichloromethane (DCM, 100 mL) and then by a mixture of DCM and methanol (1:1, 200 mL). The peptide-bound resin was dried under vacuum, transferred to a glass container, and then left in a desiccator under vacuum for 24 h.

Triethylamine (665 mL, 4.8 mmol) was added to a dispersion of the peptide bound to the resin (0.266 g, 0.1 mmol) preswollen in DMF (8 mL), and to the resultant suspension was added dropwise the *N*-hydroxysuccinimide ester of the palmitic acid (282 mg, 0.85 mmol) in DMF (8 mL). The reaction was left shaking for 24 h at 25 °C. The mixture was then concentrated under reduced pressure to remove volatile products and the residue dispersed in DMF (4 mL). The DMF suspension was filtered and the residue washed with DMF (100 mL). The product bound to the resin was treated with the reagent R (trifluoroacetic acid, ethanediol, thioanisole, anisole −90:3:5:2, 1 mL for each 0.1 mg of the resin). The reaction mixture was evaporated under vacuum, and the peptide precipitated with cold water (4 °C, 4 mL). Ethanol (20 mL) was added to wash and redissolve the precipitate, and the solution was incubated at 35 °C for 45−60 min to allow reprecipitation. The precipitate was collected by centrifugation (2500 rpm × 30 min) in a Z323 Hermle centrifuge (VWR, Poole, UK), and precipitation and centrifugation were repeated twice. The pellet was then redissolved in acetonitrile and freeze-dried.

Nanofiber Preparation. Self-assembled pDal nanofibers were prepared by vortexing a suspension of pDal (1 mg mL^{-1} for structural investigations and either 15 and 30 mg mL^{-1} for biological investigations) in water (for physical investigations) or in NaCl (0.9% w/v, for biological investigations), followed by probe sonication (MSE Soniprep 150, MSE London, UK) with the instrument set at 50% of its maximum output for 20 min.

Transmission Electron Microscopy. Samples were imaged under a Philips CM120 BioTwin transmission electron microscope (FEI Company, Eindhoven, The Netherlands). Prior to imaging, the samples were negatively stained using uranyl acetate (1% w/v) as previously described.[51,52]

Coarse-Grained Molecular Dynamics. To investigate the self-assembly and molecular organization of pDal nanofibers, coarse-grained (CG) molecular dynamics (MD) simulations were carried out using the GROMACS 4.5.1 simulation package.[53] Atomistic simulations of pDal in water were used to refine a CG model based on the MARTINI force field.[54,55] To generate the initial starting configurations for the CG simulations, 512 pDal molecules were randomly inserted (random position and orientation) into a simulation cell and then solvated with CG water particles and chloride counterions. Simulations were carried out for up to 1.6 μs. Further details of the model and the simulation parameters are provided in Supporting Information.

Linear Dichroism. LD spectra were measured with a Couette cell (Kromatek, Great Dunmow, U.K.) inserted into the sample compartment of a J-815 spectropolarimeter (Jasco UK, Great Dunmow, U.K.) adapted for LD measurements. pDal dispersions (1 mg mL^{-1} diluted to 0.2 mg mL^{-1}) were loaded onto a cylindrical quartz capillary of 3 mm internal diameter, one end of which was sealed with Araldite Rapide. A quartz rod of 2.5 mm outer diameter was suspended within the capillary and the capillary rotated within the Couette flow cell. Spectra were measured between the wavelengths of 180 and 350 nm, at a scanning speed of 100 nm min^{-1}, bandwidth of 2 nm, and an integration time of 0.5 s. Spectra were measured at a rotating speed of 1.5 V, and a nonrotating baseline spectrum was subtracted from each spectrum to account for the inherent LD signal.

X-ray Diffraction. Data sets were collected on an Oxford Diffraction Xcalibur NovaT X-ray diffractometer with the sample mounted using transmission geometry, processed, and scaled using CrysAlis^{PRO} (Oxford Diffraction, Oxford, U.K.). The dried stalk sample was mounted perpendicular to the Phi axis and rotated about Phi over 360° at 0.5°/s while exposed to Cu Kα radiation (λ = 1.5418 Å) at room temperature.

***In Vivo* Pharmacokinetics Studies.** All experiments were performed under a UK Home Office License (Animal Scientific Procedures Act 1986). Groups (n = 5) of mice [ICR (CD-1) male out bred mice (18−24 g, 4 weeks old, Harlan, Oxon, UK)] were administered either dalargin in NaCl (0.9% w/v) or pDal in NaCl at a dalargin dose of 30 mg kg^{-1} and a dose volume of 8 mL kg^{-1}. At various time points, animals were killed and their brains, livers, and plasma analyzed.

Blood samples (0.4−0.8 mL per mouse) were collected into a chilled syringe and transferred into sterile tubes spray coated with tripotassium ethylenediamine tetraacetic acid (K3, 3.6 mg) medical grade (3 × 75 mm K3E Vacutainer, PET tubes, BD Biosciences, Oxford, U.K.), and maintained on ice (4 °C) until centrifugation. Plasma was obtained after centrifugation (1600g × 15 min at 4 °C) and stored at −80 °C, until analyses could be performed. Brain and liver samples were removed, immediately frozen in liquid nitrogen, and stored at −80 °C until analyses could be performed on them.

Extraction Procedure. Plasma, brain, and liver samples were thawed, organs weighed, and water (2 mL g^{-1}) added to brains and livers. Brains and livers were homogenized. To plasma samples (50 μL) and organ homogenates (100 μL) were added ethanol (50 μL) and acetonitrile and ammonium acetate 10 mM (80:20, 250 μL) containing Aricept (10 ng mL^{-1}) as internal standard. Samples were vortexed for 20 min and centrifuged (2465g × 15 min at 4 °C), and the supernatant was subjected to liquid chromatography−mass spectrometry (LC−MS) analysis.

LC−MS analysis was carried out on a mass spectrometer instrument (Applied Biosystems API4000, Warrington, U.K.). Mode of operation: positive-ion/turbo ionspray, source temperature = 625 °C; software version, Analyst 1.4.2; multiple reaction monitoring transitions for dalargin = 726.6 → 136.2, palmitoyl dalargin = 964.8 → 136.2, D-alanine^2-leucine-enkephalin = 570.4 → 136.1; pump instrument type, JASCO XLC; HPLC column (type/size): Thermo Gold (Aqua) 30 × 3 mm, pore size = 3 mm, column temp = 50 °C, flow rate = 1.0 mL min^{-1}; volume split from LC into source, no split; run time = 2.5 min, injection volume = 20 μL. Samples were eluted with a gradient at (solvent A) 10 mM ammonium acetate, (solvent B) methanol (time = 0 min, solvent B 20%; time = 0.8 min, solvent B 90%; time = 1.8 min, solvent B 90%; time = 1.81 min, solvent B 20%). Autosampler instrument type: Research PAL CTC autosampler.

Multimodal Nonlinear Microscopy. The brains were fixed in a neutral buffered formalin solution containing formaldehyde (4% w/v) and were stored at 4−6 °C prior to experimentation. Coronal sections were cut using a mouse brain slicer matrix (Zivic Instruments, Pittsburgh, PA, USA) with 0.5 mm slice spacing intervals; the brain slices were briefly immersed in phosphate buffered saline prior to plating onto cleaned glass coverslips. Each brain section was surrounded by strips of parafilm two layers thick, which acted as spacers before the sample was covered with a second glass coverslip. Using a point heat source applied to the top coverslip, the parafilm spacers were heated to their melting temperature of 60 °C to form a water-tight seal around the brain slice, at a distance sufficiently far from the sample to prevent damage.

Imaging was performed using a custom-built multimodal nonlinear optical microscope that provided three complementary contrast mechanisms simultaneously: (1) coherent anti-Stokes Raman scattering (CARS) to detect the pDal nanofibers, (2) stimulated Raman scattering (SRS) to delineate the cellular structures within the brain, and (3) nonlinear photothermal lensing (NL-PTL), derived from hemoglobin to delineate blood vessels. For a detailed technical description of the microscope, see ref 56.

(1) Epi-detected coherent anti-Stokes Raman scattering (E-CARS) to locate the pDal nanofibers: CARS is a four-wave mixing process in which two laser beams, a pump and a Stokes beam, at frequencies ω_s and ω_p, respectively, are focused into a sample. Matching the difference in frequency ($\omega_p - \omega_s$) to that of a Raman-active molecular vibration of the chemical species of interest resonantly leads to the generation of a strong anti-Stokes signal (ω_{as}) at frequency ($\omega_{as} = 2\omega_p - \omega_s$) when the chemical species of interest is present in the sample volume. E-CARS is particularly suited to locating polymer nanomaterials within biological tissues.[37] The signal scales quadratically with the number of vibrational modes within the sample volume and therefore favors detection of polymer particles with high bond repetition. Moreover, when detected in the epi-direction, the phase-matching criteria enhance the CARS signal from

subwavelength objects while suppressing that emitted from surrounding "bulk" objects. In the case of the pDal nanofibers, strong contrast could be achieved by tuning $\omega_p - \omega_s$ to 2855 cm^{-1}, the CH_2 vibrational mode that is abundant in the palmitoyl group.

(2) Stimulated Raman scattering (SRS) to delineate cellular structures and blood-brain barrier: SRS was performed using the same pump and Stokes beams (ω_p and ω_s) to excite chemical bonds of interest; however, in SRS, amplification of the Raman signal is achieved by virtue of stimulated excitation. The intensity of the Stokes beam, I_S, experiences a gain, ΔI_S (stimulated Raman gain, SRG), and the intensity of the pump beam, I_p, experiences a loss, ΔI_p (stimulated Raman loss, SRL). Imaging is achieved by recording the SRL signal ΔI_p, which scales linearly with the concentration of a vibrational mode.

(3) Nonlinear photothermal lensing (NL-PTL) to provide contrast of the red blood cells within the brain vasculature. For the purpose of locating the blood-brain barrier, we made use of NL-PTL that results from the strong optical absorption band of hemoglobin. NL-PTL is achieved using the pump and Stokes beams and also leads to a loss in the intensity of the pump beam, ΔI_p. However, due to the thermal time taken for the thermal gradient to build up, the NL-PTL signal occurs with a phase delay with respect to the SRL signal, which can be isolated using phase-sensitive detection.

Anti-nociception Experiments. Groups ($n = 5$) were administered either NaCl (0.9% w/v), dalargin, or pDal dispersed in NaCl (0.9% w/v). Animals received a 15 mg kg^{-1} dalargin dose. Anti-nociception was assessed in mice using the tail flick warm water bioassay. The protruding distal half of the tail (4−5 cm) of mice, which were held in a tube restrainer, was immersed in circulating warm water maintained at 55 ± 0.1 °C[28] by a thermostatically controlled water bath (W14, Grant Instruments, Cambridge Ltd., Herts, U.K.). The temperature was also checked using a thermometer (Gallenkamp, Griffin, THL-333-020L, 76 mm × 1 mm, U.K.) before the start of the experiment. The response latency times, recorded for each mouse to withdraw its tail by a "sharp flick", were recorded using a digital stopwatch capable of measuring 1/100th of a second. The first sign of a rapid tail flick was taken as the behavioral end point. The baseline latency was measured for all animals prior to dosing, and animals not responding within 5 s were excluded from further testing. An analgesic responder was defined as one whose response tail flick latency was two or more times the value of the baseline latency.

Conflict of Interest: The authors declare no competing financial interest.

Acknowledgment. The School of Pharmacy is acknowledged for a scholarship to M.M. R.N. acknowledges Advantage West Midlands and the Higher Education Funding Council for England for the provision of a Science City Research Alliance Fellowship and the Centre for Scientific Computing, University of Warwick, and the U.K. National Grid Service for computational facilities to carry out this work. The linear dichroism equipment was provided by BBRSC Grant BB/F011199/1.

Supporting Information Available: Further details of the molecular dynamics simulation methodology and analysis of the molecular structure of the simulated pDal nanofibers is available. Further information on the CARS microscopy methodology is also available. This material is available free of charge *via* the Internet at http://pubs.acs.org.

REFERENCES AND NOTES

1. Lalatsa, A.; Schätzlein, A. G.; Uchegbu, I. F., Drug Delivery across the Blood Brain Barrier. In *Comprehensive Biotechnology 2nd ed.*, MurrayMoo-Young, M.; Butler, M.; Webb, C.; Moreira, A.; Grodzinski, B.; Cui, Z., Eds. Elsevier: Amsterdam, 2011; pp 657−668.
2. Carter, M. D.; Simms, G. A.; Weaver, D. F. The Development of New Therapeutics for Alzheimer's Disease. *Clin. Pharmacol. Ther.* **2010**, *88*, 475–486.
3. Brasnjevic, I.; Steinbusch, H. W.; Schmitz, C.; Martinez-Martinez, P. Delivery of Peptide and Protein Drugs over the Blood-Brain Barrier. *Prog. Neurobiol.* **2009**, *87*, 212–251.
4. Hughes, J.; Smith, T. W.; Kosterlitz, H. W.; Fothergill, L. A.; Morgan, B. A.; Morris, H. R. Identification of Two Related Pentapeptides from the Brain with Potent Opiate Agonist Activity. *Nature* **1975**, *258*, 577–580.
5. Mathers, C. D.; Loncar, D. Projection of Global Mortality and Burden of Disease from 2002 to 2030. *Plos Med.* **2006**, *3*, 2011–2030.
6. Pardridge, W. M. Drug Targeting to the Brain. *Pharm. Res.* **2007**, *24*, 1733–1744.
7. Beduneau, A.; Hindre, F.; Clavreul, A.; Leroux, J. C.; Saulnier, P.; Benoit, J. P. Brain Targeting Using Novel Lipid Nanovectors. *J. Controlled Release* **2008**, *126*, 44–49.
8. Pardridge, W. M.; Boado, R. J. Delivery of Pharmaceutical Agents *via* the Human Insulin Receptor; U.S. Patent 7,388,079, 2008.
9. Regina, A.; Demeule, M.; Che, C.; Lavallee, I.; Poirier, J.; Gabathuler, R.; Beliveau, R.; Castaigne, J. P. Antitumour Activity of ANG1005, a Conjugate between Paclitaxel and the New Brain Delivery Vector Angiopep-2. *Br. J. Pharmacol.* **2008**, *155*, 185–197.
10. Mazza, M.; Uchegbu, I. F.; Schatzlein, A. G. Cancer and the Blood-Brain Barrier: `Trojan Horses' for Courses? *Br. J. Pharmacol.* **2008**, *155*, 149–151.
11. Bihorel, S.; Camenisch, G.; Lemaire, M.; Scherrmann, J. M. Modulation of the Brain Distribution of Imatinib and Its Metabolites in Mice By Valspodar, Zosuquidar and Elacridar. *Pharm. Res.* **2007**, *24*, 1720–1728.
12. Deeken, J. F.; Loscher, W. The Blood-Brain Barrier and Cancer: Transporters, Treatment, and Trojan Horses. *Clin. Cancer Res.* **2007**, *13*, 1663–1674.
13. Kreuter, J.; Ramge, P.; Petrov, V.; Hamm, S.; Gelperina, S. E.; Engelhardt, B.; Alyautdin, R.; von Briesen, H.; Begley, D. J. Direct Evidence that Polysorbate-80-Coated Poly(butylcyanoacrylate) Nanoparticles Deliver Drugs to the CNS *via* Specific Mechanisms Requiring Prior Binding of Drug to the Nanoparticles. *Pharm. Res.* **2003**, *20*, 409–416.
14. Adenot, M.; Merida, P.; Lahana, R. Applications of a Blood-Brain Barrier Technology Platform To Predict CNS Penetration of Various Chemotherapeutic Agents. *Chemotherapy* **2007**, *53*, 73–76.
15. Fleming, A. B.; Saltzman, W. M. Pharmacokinetics of the Carmustine Implant. *Clin. Pharmacokinet.* **2002**, *41*, 403–419.
16. Debinski, W.; Tatter, S. B. Convection-Enhanced Delivery To Achieve Widespread Distribution of Viral Vectors: Predicting Clinical Implementation. *Curr. Opin. Mol. Ther.* **2010**, *12*, 647–653.
17. Takeda, T.; Saitoh, M.; Takeda, S. Solitary Cystic Brain Metastasis of Small-Cell Lung Carcinoma Controlled by a Stereotactically Inserted Ommaya Reservoir. *Am. J. Med. Sci.* **2009**, *337*, 215–217.
18. Jolliet-Riant, P.; Tillement, J. P. Drug Transfer Across the Blood-Brain Barrier and Improvement of Brain Delivery. *Fundam. Clin. Pharmacol.* **1999**, *13*, 16–26.
19. Hansen, D. W.; Stapelfeld, A.; Savage, M. A.; Reichman, M.; Hammond, D. L.; Haaseth, R. C.; Mosberg, H. I. Systemic Analgesic Activity and Delta-Opioid Selectivity in 2,6-Dimethyl-Tyr1,D-Pen2,D-Pen5 Enkephalin. *J. Med. Chem.* **1992**, *35*, 684–687.
20. Weber, S. J.; Greene, D. L.; Sharma, S. D.; Yamamura, H. I.; Kramer, T. H.; Burks, T. F.; Hruby, V. J.; Hersh, L. B.; Davis, T. P. Distribution and Analgesia of H-3 D-Pen2,D-Pen5 Enkephalin and 2-Halogenated Analogs after Intravenous Administration. *J. Pharmacol. Exp. Ther.* **1991**, *259*, 1109–1117.
21. Bodor, N.; Prokai, L.; Wu, W. M.; Farag, H.; Jonalagadda, S.; Kawamura, M.; Simpkins, J. A Strategy for Delivering Peptides into the Central Nervous System by Sequential Metabolism. *Science* **1992**, *257*, 1698–1700.
22. Batrakova, E. V.; Vinogradov, S. V.; Robinson, S. M.; Niehoff, M. L.; Banks, W. A.; Kabanov, A. V. Polypeptide Point

Modifications with Fatty Acid and Amphiphilic Block Copolymers for Enhanced Brain Delivery. *Bioconjugate Chem.* **2005**, *16*, 793–802.
23. Egleton, R. D.; Abbruscato, T. J.; Thomas, S. A.; Davis, T. P. Transport of Opioid Peptides into the Central Nervous System. *J. Pharm. Sci.* **1998**, *87*, 1433–1439.
24. Tysseling-Mattiace, V. M.; Sahni, V.; Niece, K. L.; Birch, D.; Czeisler, C.; Fehlings, M. G.; Stupp, S. I.; Kessler, J. A. Self-Assembling Nanofibers Inhibit Glial Scar Formation and Promote Axon Elongation after Spinal Cord Injury. *J. Neurosci.* **2008**, *28*, 3814–3823.
25. Zhou, M.; Smith, A. M.; Das, A. K.; Hodson, N. W.; Collins, R. F.; Ulijn, R. V.; Gough, J. E. Self-Assembled Peptide-Based Hydrogels as Scaffolds for Anchorage-Dependent Cells. *Biomaterials* **2009**, *30*, 2523–2530.
26. Standley, S. M.; Toft, D. J.; Cheng, H.; Soukasene, S.; Chen, J.; Raja, S. M.; Band, V.; Band, H.; Cryns, V. L.; Stupp, S. I. Induction of Cancer Cell Death by Self-Assembling Nanostructures Incorporating a Cytotoxic Peptide. *Cancer Res.* **2010**, *70*, 3020–3026.
27. Pencheva, N.; Ivancheva, C.; Dimitrov, E.; Bocheva, A.; Radomirov, R. Dalargin and Cys-(O_2NH_2) (2) Analogs of Enkephalins and their Selectivity for Mu-Opioid Receptors. *Gen. Pharmacol.* **1995**, *26*, 799–808.
28. Lalatsa, A.; Lee, V.; Malkinson, J. P.; Zloh, M.; Schatzlein, A. G.; Uchegbu, I. F. A Prodrug Nanoparticle Approach for the Oral Delivery of a Hydrophilic Peptide, Leucine(5)-Enkephalin, to the Brain. *Mol. Pharmaceutics* **2012**, *9*, 1665–1680.
29. Andersen, C. B.; Hicks, M. R.; Vetri, V.; Vandahl, B.; Rahbek-Nielsen, H.; Thogersen, H.; Thogersen, I. B.; Enghild, J. J.; Serpell, L. C.; Rischel, C.; Otzen, D. E. Glucagon Fibril Polymorphism Reflects Differences in Protofilament Backbone Structure. *J. Mol. Biol.* **2010**, *397*, 932–946.
30. Krebs, M. R.; Macphee, C. E.; Miller, A. F.; Dunlop, I. E.; Dobson, C. M.; Donald, A. M. The Formation of Spherulites by Amyloid Fibrils of Bovine Insulin. *Proc. Natl. Acad. Sci. U.S.A.* **2004**, *101*, 14420–14424.
31. Ewles, M.; Goodwin, L. Bioanalytical Approaches to Analyzing Peptides and Proteins By LC-MS/MS. *Bioanalysis* **2011**, *3*, 1379–1397.
32. Rauh, M. LC-MS/MS For Protein and Peptide Quantification in Clinical Chemistry. *J. Chromatogr., B: Anal. Technol. Biomed. Life Sci.* **2012**, *883*, 59–67.
33. Kalenikova, E. I.; Dmitrieva, O. F.; Korobov, N. V.; Zhukovskii, S. V.; Tishchenko, V. A. Pharmacokinetics of Dalargin. *Vopr. Med. Khim.* **1988**, *34*, 75–83.
34. van Rooy, I.; Cakir-Tascioglu, S.; Hennink, W. E.; Storm, G.; Schiffelers, R. M.; Mastrobattista, E. *In Vivo* Methods To Study Uptake of Nanoparticles into the Brain. *Pharm. Res.* **2011**, *28*, 456–471.
35. Min, W.; Freudiger, C. W.; Lu, S. J.; Xie, X. S. Coherent Nonlinear Optical Imaging: Beyond Fluorescence Microscopy. *Annu. Rev. Phys. Chem.* **2011**, *62*, 507–530.
36. Garrett, N. L.; Lalatsa, A.; Begley, D.; Mihoreanu, L.; Uchegbu, I. F.; Schätzlein, A. G.; Moger, J. Label-Free Imaging of Polymeric Nanomedicines Using Coherent Anti-Stokes Raman Scattering Microscopy. *J. Raman Spectrosc.* **2012**, *43*, 681–688.
37. Garrett, N. L.; Lalatsa, A.; Uchegbu, I.; Schatzlein, A.; Moger, J. Exploring Uptake Mechanisms of Oral Nanomedicines Using Multimodal Nonlinear Optical Microscopy. *J. Biophotonics* **2012**, *5*, 458–468.
38. Lalatsa, A.; Garrett, N.; Moger, J.; Schatzlein, A. G.; Davis, C.; Uchegbu, I. F. Delivery of Peptides to the Blood and Brain after Oral Uptake of Quaternary Ammonium Palmitoyl Glycol Chitosan Nanoparticles. *Mol. Pharmaceutics* **2012**, *9*, 1764–1774.
39. Beniash, E.; Hartgerink, J. D.; Storrie, H.; Stendahl, J. C.; Stupp, S. I. Self-Assembling Peptide Amphiphile Nanofiber Matrices for Cell Entrapment. *Acta Biomater.* **2005**, *1*, 387–397.
40. Wagner, S.; Zensi, A.; Wien, S. L.; Tschickardt, S. E.; Maier, W.; Vogel, T.; Worek, F.; Pietrzik, C. U.; Kreuter, J.; von Briesen, H. Uptake Mechanism of ApoE-Modified Nanoparticles on Brain Capillary Endothelial Cells as a Blood-Brain Barrier Model. *PLoS One* **2012**, *7*, e32568.
41. Andrieux, K.; Couvreur, P. Polyalkylcyanoacrylate Nanoparticles for Delivery of Drugs Across the Blood-Brain Barrier. *Wiley Interdiscip. Rev.: Nanomed. Nanobiotechnol.* **2009**, *1*, 463–474.
42. Knipe, J. O.; Mosure, K. W. Nonclinical Pharmacokinetics of BMS-292655, a Water-Soluble Prodrug of the Antifungal Ravuconazole. *Biopharm. Drug Dispos.* **2008**, *29*, 270–279.
43. Sharkey, E. M.; O'Neill, H. B.; Kavarana, M. J.; Wang, H. B.; Creighton, D. J.; Sentz, D. L.; Eiseman, J. L. Pharmacokinetics and Antitumor Properties in Tumor-Bearing Mice of an Enediol Analogue Inhibitor of Glyoxalase I. *Cancer Chemother. Pharmacol.* **2000**, *46*, 156–166.
44. Cassel, J. A.; Daubert, J. D.; DeHaven, R. N. H-3 Alvimopan Binding to the Mu Opioid Receptor: Comparative Binding Kinetics of Opioid Antagonists. *Eur. J. Pharmacol.* **2005**, *520*, 29–36.
45. Maslov, L. N.; Fedorova, N. A.; Dudko, V. A.; Karpov, R. S. Effect of Peripheral Opiate Receptor Agonist Dalargin on Exercise Tolerance in Patients with Coronary and Peripheral Arteries Atherosclerosis. *Fiziol. Chel.* **2002**, *28*, 81–87.
46. Hamley, I. W.; Castelletto, V.; Moulton, C. M.; Rodriguez-Perez, J.; Squires, A. M.; Eralp, T.; Held, G.; Hicks, M. R.; Rodger, A. Alignment of a Model Amyloid Peptide Fragment in Bulk and at a Solid Surface. *J. Phys. Chem. B* **2010**, *114*, 8244–8254.
47. Maurer-Stroh Sebastian, D. M.; Kuemmerer, N.; Lopez de la Paz, M.; Martins, I. C.; Reumers, J.; Morris, K. L.; Copland, A.; Serpell, L.; Serrano, L.; Schymkovitz, J. W. H.; Rousseau, F. Exploring the Sequence Determinants of Amyloid Structure Using Position-Specific Scoring Matrices. *Nat. Methods* **2010**, *7*, 237–242.
48. Pashuck, E. T.; Stupp, S. I. Direct Observation of Morphological Transformation from Twisted Ribbons into Helical Ribbons. *J. Am. Chem. Soc.* **2010**, *132*, 8819–8821.
49. Hartgerink, J. D.; Beniash, E.; Stupp, S. I. Self-Assembly and Mineralization of Peptide-Amphiphile Nanofibers. *Science* **2001**, *294*, 1684–1688.
50. Lee, O. S.; Stupp, S. I.; Schatz, G. C. Atomistic Molecular Dynamics Simulations of Peptide Amphiphile Self-Assembly into Cylindrical Nanofibers. *J. Am. Chem. Soc.* **2011**, *133*, 3677–3683.
51. Wong, P. E.; Tetley, L.; Dufes, C.; Chooi, K. W.; Bolton, K.; Schätzlein, A. G.; Uchegbu, I. F. Polyamine Aza-Cyclic Compounds Demonstrate Anti-Proliferative Activity *in Vitro* but Fail To Control Tumour Growth *in Vivo*. *J. Pharm. Sci.* **2010**, *99*, 4642–4657.
52. Siew, A.; Le, H.; Thiovolet, M.; Gellert, P.; Schatzlein, A.; Uchegbu, I. Enhanced Oral Absorption of Hydrophobic and Hydrophilic Drugs Using Quaternary Ammonium Palmitoyl Glycol Chitosan Nanoparticles. *Mol. Pharmaceutics* **2012**, *9*, 14–28.
53. Hess, B.; Kutzner, C.; van der Spoel, D.; Lindahl, E. GROMACS 4: Algorithms for Highly Efficient, Load-Balanced, and Scalable Molecular Simulation. *J. Chem. Theory Comput.* **2008**, *4*, 435–447.
54. Marrink, S. J.; Risselada, H. J.; Yefimov, S.; Tieleman, D. P.; De Vries, A. H. The MARTINI Force Field: Coarse Grained Model for Biomolecular Simulations. *J. Phys. Chem. B* **2007**, *111*, 7812–7824.
55. Monticelli, L.; Kandasamy, S. K.; Periole, X.; Larson, R. G.; Tieleman, D. P.; Marrink, S. J. The MARTINI Coarse-Grained Force Field: Extension to Proteins. *J. Chem. Theory Comput.* **2008**, *4*, 819–834.
56. Moger, J.; Garrett, N. L.; Begley, D.; Mihoreanu, L.; Lalatsa, A.; Lozano, M.; Mazza, M.; Schatzlein, A.; Uchegbu, I. F. Imaging Cortical Vasculature with Stimulated Raman Scattering and Two Photon Photothermal Lensing Microscopy. *J. Raman Spectrosc.* **2012**, *43*, 668–674.